Optical Materials 137 (2023) 113603

Contents lists available at ScienceDirect

Optical Materials

journal homepage: www.elsevier.com/locate/optmat

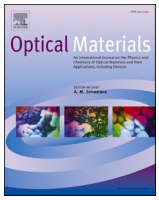

Research Article

Femtosecond nonlinear optical properties of polycyclic aromatic hydrocarbon-based Benzo[e]pyrene derivatives

Sudhanshu Kumar Nayak [a,1], Ranjith Kore [b,1], Md Soif Ahmed [a], Pankaj Verma [c], Rohini Vallavoju [b], Dipanjan Banerjee [d], Someshwar Pola [b], Venugopal Rao Soma [d], Prabhakar Chetti [c], Sai Santosh Kumar Raavi [a,e,*]

[a] Ultrafast Photophysics and Photonics Laboratory, Department of Physics, Indian Institute of Technology Hyderabad, Kandi, 502285, Telangana, India
[b] Department of Chemistry, Osmania University, Hyderabad, 500007, Telangana, India
[c] Department of Chemistry, National Institute of Technology Kurukshetra, 136119, India
[d] Advanced Centre of Research in High Energy Materials (ACRHEM), DRDO Industry Academia – Centre of Excellence (DIA-COE) University of Hyderabad, Hyderabad 500046, Telangana, India
[e] Department of Climate Change, Indian Institute of Technology Hyderabad, Kandi, 502285, Telangana, India

ARTICLE INFO

Keywords:
Ultrafast nonlinearity
Z-scan technique
TDDFT
Optical limiting onset
Second hyperpolarizability

ABSTRACT

We herein report our results on the nonlinear optical (NLO) properties of three polycyclic aromatic hydrocarbons (PAHs) based benzo[e]pyrene derivatives namely 10-phenylbenzo[e]pyrene (BP1), 13-fluoro-10-(4-fluorophenyl)benzo[e]pyrene (BP2), and 13-methoxy-10-(4 methoxyphenyl)benzo[e]pyrene (BP3). Using experimental techniques such as UV–Visible absorption, Z-scan technique, and theoretical time-dependent density functional theory (TDDFT), we have investigated the linear absorption, NLO coefficients, second hyperpolarizability, and optical limiting onset of these molecules. The ultrafast nonlinear Z-scan experiment was performed using ~70 fs pulsed laser with 800 nm as central wavelength. Using the three-level model analysis based on rate equations, the contribution of different nonlinear processes contributing to nonlinear absorptions in these molecules is elucidated. All three molecules exhibited strong reverse saturable absorption due to mixed contribution of two-photon absorption (2PA) and three-photon absorption (3PA) with 2PA and 3PA coefficients of (1.26–1.79) $\times 10^{-11}$ cm/W and (6.23–7.39) $\times 10^{-5}$ cm^3/GW^2, respectively. The closed-aperture Z-scan data for all the examined molecules depicted valley-peak signature, which indicated a positive refractive index. The second hyperpolarizability was calculated with magnitude observed ~10^{-32} esu. Using the TDDFT calculation, the complete optimization of the individual structure of molecules was achieved and the results matched with experimental observations.

1. Introduction

Nonlinear optics (NLO) is contemplated as the most promising field with emerging applications in the field of photonics, optoelectronics, and biomedicine [1–7]. Both inorganic [8] and organic [9–11] materials exhibit strong NLO properties, which play a good role in manipulating optical signals in the domain of telecommunications and other optical signal processing applications. By changing small modifications in the chemical structure of organic material, the NLO properties can be easily tunable. Further, in the case of integrated components, the polymer-based materials having significant third-order NLO properties play an important role in the manipulation of optical information. The material with extended π-conjugation exhibits an electro-optic effect that refractive index of the material changes with application of electric field. Due to their good NLO property, there are emerging applications in the fields of optical limiting, optical switching, optical modulation, data storage, and optical computing [12–14]. Over the last two decades, several researchers have investigated the promising optoelectronic applications of affordable, easily synthesized, merge frameworks of polycyclic aromatic hydrocarbons (PAHs) materials. These materials have

* Corresponding author. Ultrafast Photophysics and Photonics Laboratory, Department of Physics, Indian Institute of Technology Hyderabad, Kandi, 502285, Telangana, India.
E-mail address: sskraavi@phy.iith.ac.in (S.S.K. Raavi).
[1] Equal Contribution

https://doi.org/10.1016/j.optmat.2023.113603
Received 21 November 2022; Received in revised form 31 January 2023; Accepted 16 February 2023
Available online 26 February 2023

good properties such as easy solubility, thermal stability, and photostability with schematic preparation [15,16]. Even though, these materials are limited in extent to their synthesis method and photoemission properties, they have numerous applications in the field of organic molecule based electronics and are also used to construct substances in optoelectronics [17]. A literature survey exposed that various class of PAHs signifying optical and NLO properties [18,19]. As these molecules show good multiphoton absorption properties, so they have fascinated consideration in the field of NLO research. Organic molecules having prolonged π-conjugation showing admirable NLO, photoluminescence, and single-photon absorption process being broadly involved in the two-photon photodynamic behavior [20], 3-D optical data storage [21] and light-emitting diodes [22]. The proposed PAHs based molecules with appropriate ordering of π-conjugation that play a significant role in refining NLO retaliation, based upon their extended π-electronic delocalization and improved donor (D) to acceptor (A) intramolecular transfer of charge through π-spacers [23,24]. Due to the presence of conjugated π-electron A and D tail groups asymmetrically which may cause to expand their electron-donating or -accepting stability, leads to improved absorption properties. Their schematic synthesis and structural difference have been recognized as suitable key elements in the organic π-conjugated molecules used in the NLO-based devices. This type of molecules with proper geometric framework, one or two-photon absorption features, thermodynamic properties, and energy levels have been examined and also achieved promising excellent outcomes, signifying that those molecules have capabilities like NLO materials [25].

Benzo-pyrenes (BPs) molecules, which are molecular frameworks of pyrene, have currently been investigated for such properties because of their strong and electronically adjustable π-system [26]. The 4,5-diphenylphenanthro [4,5-abc]phenazine type of materials consists of phenazine moiety that is communicated to enhance solubility and as an attaching group for designated properties, but the various substituents on the nitrogen have small effect on the optoelectronic applications. A well-organized plan to tune the optical and photophysical properties of the pyrene-based required cooperating on their solubility 5,6- position substitution on pyrene core [27]. Pyrene basic-expansion, i.e., mounting the π-conjugated part around the pyrene framework, is another probable way to accomplish molecular scaffolds with adjustable photophysical properties for current applications [28,29].

In this work, we present the linear, ultrafast NLO, and photophysical properties of a new class of pyrene-based PAHs molecules denoted as BP1, BP2, and BP3, synthesized via visible light irradiation conditions [30,31]. Additionally, we have calculated the HOMO-LUMO energy level of these molecules and estimated the absorption properties and second hyperpolarizability using DFT/TDDFT method.

2. Experimental methods

All the synthesis processes for the synthesis of the intermediate compounds using earlier method are shown in the electronic supplementary information (SI) [32]. The final molecules are obtained in the presence of Ag–ZnO NPs and visible light irradiation process with good yields.

The steady-state absorption of these molecules was measured by using a UV–Vis absorption spectrometer. The steady-state photoluminescence (PL) spectra were measured by FLS-1000 spectrometer (Edinburg instrument) by dissolving the samples in dichloromethane (DCM) solvent. The dilute solutions were placed inside a 1 mm quartz cuvette in the special sample holder. The TRPL (Time-Resolved Photoluminescence) was measured by the time-correlated single-photon counting (TCSPC) technique [33] using FLS-1000 picosecond (ps) diode laser of 405 nm wavelength and the PL decay times were fitted by using 'Fluoracle' software. The instrument response function (IRF) was measured by using Ludox solution. The TRPL data were fitted by re-convolution fit with IRF data and the χ^2 values determined the quality of the fits.

The characterization of all nonlinear properties of materials was performed using the conventional Z-scan setup, discussed elsewhere [34–37]. In this experiment, an ultrafast femtosecond laser with an excitation wavelength of 800 nm was used as the excitation source. This excitation beam has been collected from Ti: sapphire laser pulse from an amplifier (Libra, M/s Coherent) with ≈70 fs pulse duration and 1 kHz repetition frequency at a central wavelength of 800 nm. The beam was focused by a biconvex lens of 15 cm focal length producing intensity at the focus of ≈189 GW/cm^2 on the sample (of concentration ~ 10^{-4} M), which was placed inside the quartz cuvette of 1 mm path length aligned along the laser beam direction. The sample was scanned from -z to + z (z is the position of the sample) using a motorized stage interface. The transmitted beam was collimated and focused by another lens which used for collecting the divergent outcome beam. The transmitted beam from the sample was detected by the silicon photodiode (PD-Thorlabs). The nonlinear absorption cross-section is investigated using Open-aperture (OA) Z-scan and nonlinear refractive index as well as second hyperpolarizability is estimated using Closed-aperture (CA) Z-scan. Both the power sensor and motorized stage were interfaced by the LABVIEW SOFTWARE, monetarized by the computer.

3. Results and discussions

3.1. Photophysical studies

The absorption spectra of these molecules were measured using the UV–Vis absorption spectrometer as shown in Fig. 1. (a). There are various kind of solvents like dichloromethane (DCM), dichlorobenzene (DCB), and dichloroethane (DCE) in which those molecules are soluble and useful for photophysical characterization. In our case, for comparative study purposes, we have prepared each solution at the same concentration (~10^{-4} M) using DCM as solvent. From absorption measurement, the absorption for BP1, BP2, and BP3 are at 375 nm, 370 nm, and 363 nm, respectively with 290 nm (max), summarized in Table 1. There is no significant absorption in the 800 nm wavelength region, shown in Fig. S1(a) (supplementary information).

The absorption peaks of these molecules present at the lower wavelength region are due to the π-π* intermolecular transitions [38]. The emission properties of the molecules in DCM solvent are studied at room temperature by exciting the molecules at $\lambda_{ex} = 380$ nm excitation, as all molecules show absorption in that region. As we have done the comparative study, we have fixed all the experimental parameters for these measurements. The photoluminescence spectra of those molecules are observed with an excitation of 380 nm wavelength, shown in Fig. 1. (b). The emission peaks are given in Table 1. The maximum emission for BP1, BP3 at $\lambda_{max}^{em} = 420$ nm, 430 nm. Whereas, in the case of BP2 the main emission at 414 nm, 431 nm. There is another broadened peak nearly at 544 nm and 554 nm for BP1 and BP2, respectively. These bands may be originated due to the presence of excited states having a twisted aryl unit connected with the aromatic core and the relaxed form to the low-energy and planar form. In methoxy-based pyrene molecule (BP3), it acts as a good donor which restricts the relaxation to the planar excited state. This similar kind of features have shown by DBP molecules [32].

To get more insight into the absorption properties, all the molecules are optimized at B3LYP/6-31G (d, p) level of the theory by using Gaussian 16W [39] software. These optimized structures have zero imaginary frequencies, which indicates that all the optimized structures are located at the bottom-most point of the potential energy surface. The optimized structures of all the molecules with their dihedral angles are listed in Table S3. The absorption properties are estimated using time-dependent density functional theory (TDDFT). The evaluated oscillator strength (f), absorption maximum (λ_{max}), major transitions (M. T.), and % weight contribution (%Ci) for all the molecules are shown in Table 2. The absorption values of the three molecules are shown from 329 nm to 407 nm given in Table 2. Absorption maximum for BP1 is 390

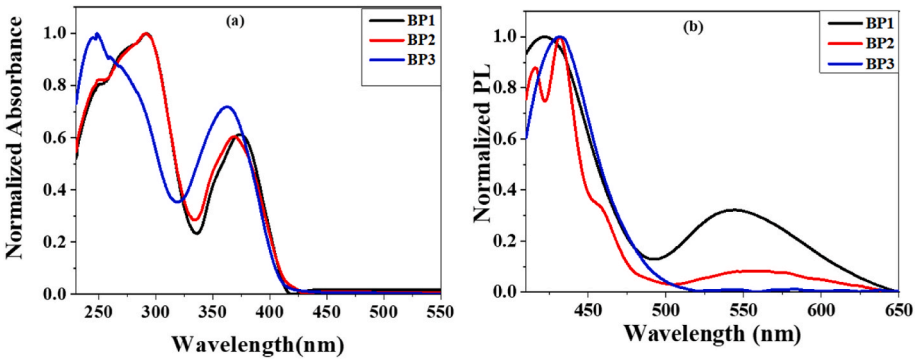

Fig. 1. (a) UV–visible absorption spectra and (b) PL spectra at λ_{ex} = 380 nm of BP1, BP2, BP3.

Table 1
Absorption & emission data of BP1, BP2, and BP3.

Sample	Absorption λ_{max}^{abs} (nm)	Photoluminescence λ_{max}^{em} (nm)
BP1	375, 290	420
BP2	370, 290	431
BP3	363	430

Table 2
Absorption maxima (λ_{max} in nm), oscillator strength (*f*), major transition (M.T.), and (%Ci > 10) obtained at TD-B3LYP method using 6-31G (d, p) basis sets.

Name	States	λ_{max} (nm)	f	M.T.	%Ci
BP1	S1	390	0.254	H→L	95
	S2	362	0.000	H-1→L	48
				H→L+1	49
	S3	329	0.007	H-2→L	41
				H→L+2	52
BP2	S1	392	0.242	H→L	93
	S2	363	0.009	H-1→L	41
				H→L+1	50
	S3	332	0.029	H-2→L	27
				H-1→L	17
				H→L+2	45
BP3	S1	407	0.271	H→L	94
	S2	365	0.019	H-1→L	34
				H→L+1	54
				H-2→L	14
	S3	340	0.009	H-1→L	20
				H→L+2	49

nm and, with the replacement of two H atoms with fluorine atoms, shows no considerable shift in absorption maxima (BP2 = 392 nm). Further, the replacement of two fluorine atoms with two methoxy groups show a red shifted absorption (BP3 = 407 nm). All the molecules show the main transition from HOMO to LUMO with high oscillatory strength and other excitations arising due to mixed transitions. The absorption spectra of BP1, BP2, and BP3 are shown in Fig. S1(b).

The pictures of frontier molecular orbital (FMO's) those are HOMO and LUMO for all the molecules are shown in Fig. 2. The distribution of electron density of HOMO and LUMO are spread over the backbone of the compounds, as shown in Fig. 2. The calculated HOMO, LUMO energies and HOMO-LUMO energy Gap (HLG) are tabulated in Table 3. The calculated HOMO energies for BP1, BP2 and BP3 are −5.15, −5.28 and −4.90 eV respectively. The LUMO energies for BP1, BP2 and BP3 are −1.67, −1.80 and −1.53 eV respectively. The order of calculated HOMO-LUMO gap (HLG) is BP1 = BP2 > BP3. There is a decrease in HOMO-LUMO energy gap as we move from BP1 to BP3 due to more destabilization of HOMO, shown in Fig. 2.

Time-resolved photoluminescence (TRPL) of those molecules was observed by using the TCSPC technique shown in Fig. 3. Here, the decay lifetimes for the molecules are acquired from the biexponential fit. The

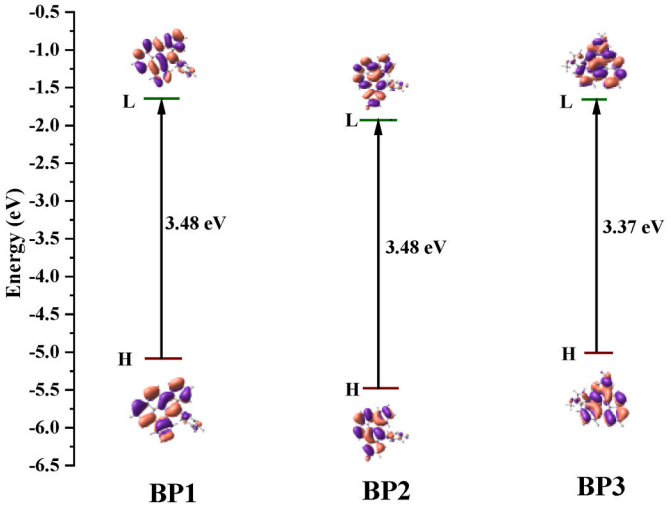

Fig. 2. The electronic transitions occurring in all isomers calculated at TD-B3LYP method using 6-31G (d, p) basis sets.

Table 3
HOMO, LUMO and HOMO-LUMO gap.

Names	HOMO (eV)	LUMO (eV)	HOMO-LUMO gap (eV)
BP1	−5.15	−1.67	3.48
BP2	−5.28	−1.80	3.48
BP3	−4.90	−1.53	3.37

observed data are in the nanosecond (ns) regime with τ_1 and τ_2 in the range of (3.05–3.26) ns and (5.50–7.92) ns., and the extracted parameters are presented in Table 4.

3.2. Ultrafast nonlinear optical studies

To investigate the NLO properties of those organic molecules, we have performed the Z-scan experiment. From this technique, the multi-photon absorption coefficient, third-order nonlinear susceptibility, and second hyperpolarizability of those three molecules were evaluated. In the Z-scan method, we have measured the transmittance of nonlinear media as the function of the position of sample 'z' with and without keeping an aperture in the far-field [40]. When the variation of the beam diameter is negligible inside the sample due to either nonlinear refraction or diffraction, then the sample is typically considered as 'thin' sample. In that case, the self-refraction process is regarded as 'external self-action' [34,41,42]. There are two criteria for the sample to behave as 'thin' sample: (1) For nonlinear diffraction, the length of the sample should be much less than Rayleigh length $L \ll z_0$, (2) for nonlinear

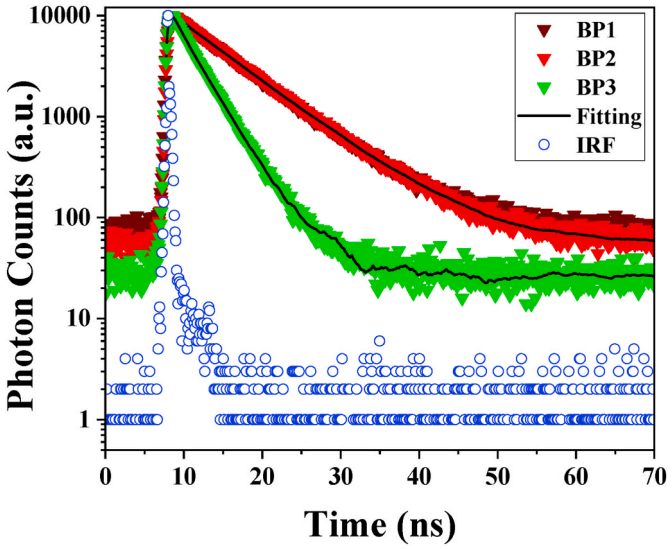

Fig. 3. TRPL data of BP1, BP2, and BP3 using TCSPC. The scattered points and the solid black line correspond to experimental points and theoretical fits, respectively.

Table 4
Estimated TRPL data of BP1, BP2, and BP3 from our experiment.

Sample	τ_1 (ns)	rel %	τ_2 (ns)	rel %	χ^2
BP1	3.26	82.10	7.79	17.90	1.25
BP2	3.25	79.34	7.92	20.66	1.20
BP3	3.05	88.64	5.50	11.36	1.16

refraction $L \ll z_0/\Delta\Phi$, where $\Delta\Phi$ is the maximum phase shift due to nonlinearities of the sample [34]. The intensity of the Gaussian laser beam is given by the formula [43]

$$I(z,r) = \frac{I_0}{1+(z/z_0)^2} \exp\left(\frac{-2r^2}{\omega^2(z)}\right) \exp\left(-\frac{t^2}{\tau_p{}^2}\right) \quad (1)$$

where I_0 is the peak intensity of the focused beam at the focus, z stands for sample distance from z = 0, and $z_0 = \frac{\pi\omega_0{}^2}{\lambda}$ represents the Rayleigh length with $\omega_0 = \frac{2f\mathrm{D}}{\pi\lambda}$ as the beam waist at the focus, f marks the focal length of the lens, D is the diameter of the laser beam, λ denotes the wavelength of the laser beam, and ω(z) indicates the beam waist at a different position (z) of sample is given by

$$\omega(z) = \omega_0\left(1+(z/z_0)^2\right)^{1/2} \quad (2)$$

The Z-scan method is of two types (i) Open-aperture (OA) and (ii) Closed-aperture (CA), depending on placing without or with an aperture in front of the detector, respectively.

3.2.1. Open-aperture (OA) Z-scan

In the OA Z-scan process, no aperture was placed in front of the detector. Multiphoton absorption (MPA) refers to a variety of numerous effects that deal with only one of the properties of requiring the destruction of two or more quanta of the incident laser light in this process [44]. MPA may be two-photon absorption (2PA) or three-photon absorption (3PA) depending upon the number of quanta (2 or 3) required to excite the electron from the ground state to the excited state through virtual intermediate states. Therefore, multiphoton absorption coefficients can be calculated whether the sample undergoes with 2PA, 3PA process. This 2PA, 3PA, represent the form of reverse saturable absorption (RSA). This is the type of nonlinear process in which absorption of the excited state is larger than absorption of the ground state.

Fig. 4 (a-c) shows the OA Z-scan data in which the experimental data shows RSA features, that the transmittance decreases near to focus (z = 0) with increasing intensity. So, the molecules undergo MPA processes. In order to understand the contribution of MPA processes, we have performed the three-level modelling for these organic molecules interacting with ultrashort pulsed laser of pulse duration ~70 fs with ignoring the triplet states, as intersystem crossing rates are very slower (~few hundreds of picoseconds) [45]. In the three-level fitting, N_0, N_1, and N_2 correspond to the population numbers in S_0, S_1, and S_n state, respectively. From Table S2, electrons will be move to S_1 due to 2PA and move to higher excited state above to S_1 due to 3PA. Equations (3(a)-(d)) describe the processes that leads to the nonlinear absorption in benzo[e] pyrene organic molecules having S_0, S_1, and S_n singlet states. For better fitting, we have included both 2PA and 3PA processes in the three-level model. We have considered the processes that incorporated with the nonlinear absorptions, those are (a) two-photon absorption coefficient (β), (b) three-photon absorption coefficients (α_3). The contributions from all these nonlinear processes leads to RSA, which were found with solving the differential rate equations governs the populations in three energy levels.

$$\frac{dN_0}{dt} = -\frac{\sigma_0 N_0 I}{\hbar\omega} - \frac{\beta I^2}{2\hbar\omega} - \frac{\alpha_3 I^3}{3\hbar\omega} + \frac{N_1}{\tau_{S1}} \quad (3a)$$

$$\frac{dN_1}{dt} = \frac{\sigma_0 N_0 I}{\hbar\omega} + \frac{N_2}{\tau_{Sn}} - \frac{N_1}{\tau_{S1}} \quad (3b)$$

$$\frac{dN_2}{dt} = \frac{\beta I^2}{2\hbar\omega} + \frac{\alpha_3 I^3}{3\hbar\omega} - \frac{N_2}{\tau_{Sn}} \quad (3c)$$

And the intensity of pulse that transmitted through the sample can be calculated by using relation

$$\frac{dI}{dz} = -\sigma_0 N_0 I - \beta I^2 - \alpha_3 I^3 \quad (3d)$$

where, $I = I_{00} \times \frac{\omega_0^2}{\omega^2(z)} \times \exp\left(-\frac{t^2}{\tau_p^2}\right) \times exp\left(-\frac{2r^2}{\omega^2(z)}\right)$ and

$$\omega(z) = \omega_0\left\{1+\left(\frac{z}{z_0}\right)^2\right\}^{1/2}.$$

In these above equations, σ_0 represents the ground state (S_0) absorption cross-sections. τ_{S1} and τ_{Sn} represent the lifetimes of S_1 and S_n states, respectively. τ_p denotes the pulse duration with z_0, ω_0 are the Rayleigh range and the beam waist at the focus, respectively. The intensity (I) is a function of r, t, z, and I_{00} is the intensity of Gaussian laser beam at the focus. These coupled differential equations are first decoupled and then integrate over time, length, along radial direction (r) before solving numerically them using Runge-Kutta 4th order method [45–47]. Assuming the input laser beam as Gaussian in nature, the different integrating limits for r, t, z are varied from (0 to ∞) , (-∞ to + ∞) and (0 to L), respectively, where L be the length of the sample. The number slices for r, t, and z are 40, 20, and 10, respectively. Then from the least square fitting of experimental data β, and α_3 can be evaluated. The lifetimes for the fitting equations are derived from the TRPL data shown in Fig. 3. The samples are decaying with double exponential manner, generally we have used the decay lifetime (>80% weight) of the BP1, BP2, and BP3 as mentioned in Table 4. We are taking only large weight decay lifetime for fitting the data with ~70 fs laser pulse excitations, since both the lifetimes are not affecting significantly [45]. The best fitting was observed by including the contribution of both 2PA (β) and 3PA (α_3) in the rate equations. The data plotted with an error bar of ~ ±10% for inaccuracies in the collection of data. The errors included for fitting the data, calculation of peak intensity, measuring the beam diameter of incident laser at before the sample, and calibration for the intensity cut-off filters used. The extracted values of nonlinear parameters are given in Table 5.

The ground state absorption cross-section (σ_0)= (α/N), where α is the

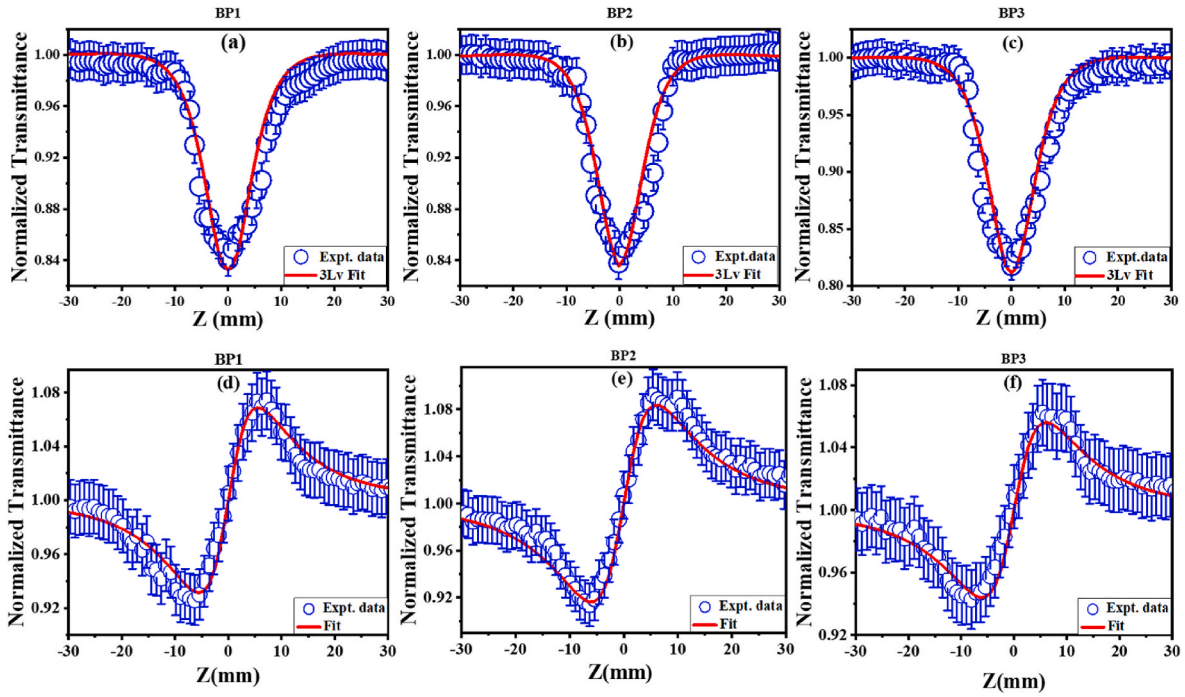

Fig. 4. Open-aperture Z-scan data of (a) BP1, (b) BP2, (c) BP3; Closed-aperture Z-scan data of (d) BP1, (e) BP2, (f) BP3.

Table 5
Estimated NLO Coefficients of BP1, BP2, and BP3 from Z-scan experiment.

Sample	$n_2 \times 10^{-16}$ (cm^2/W)	$\lvert\chi^3\rvert \times 10^{-14}$ (esu)	$\gamma \times 10^{-32}$ (esu)	DFT-derived $\gamma \times 10^{-32}$ (esu)	$\beta \times 10^{-11}$ (cm/W)	$\alpha_3 \times 10^{-5}$ (cm^3/GW^2)	$\sigma_3 \times 10^{-77}$ (cm^6s^2/photon^2)
BP1	2.31	1.18	2.44	−0.12	1.26	6.23	1.6
BP2	2.79	1.43	2.96	−0.12	1.37	6.57	1.7
BP3	1.87	1.0	1.97	−0.14	1.74	7.39	1.9

linear absorbance of sample and N is the number density of molecule per cm^3. The value of σ_0 for BP1, BP2, and BP3 are 5.72×10^{-18} cm^2, 2.81×10^{-18} cm^2, 1.42×10^{-18} cm^2 respectively. The 2PA cross-section for BP1, BP2, and BP3 were calculated with value 1.3×10^{-47} cm^4 s/photon, 1.41×10^{-47} cm^4 s/photon, and 1.84×10^{-47} cm^4 s/photon respectively. The 3PA cross-section is given by the formula [36]

$$\sigma_3 = \frac{(\hbar\omega)^2}{N}\alpha_3, \tag{4}$$

where ω and α_3 denote the frequency of the fs laser radiations and 3PA coefficients, respectively. The 3PA cross-sections for those molecules were estimated to be in the range $(1.3–1.9) \times 10^{-77}$ cm^6s^2/photon^2 and given in Table 5. From fitting, it was observed that, the experimental data were fitted well with the theoretical modelling by considering both β and α_3 in the rate equations. From the DFT calculations, it was observed that for BP1, BP2, and BP3 the oscillator strengths at 400 nm (corresponds to 2PA coefficient) are 0.254, 0.242 and 0.271, respectively and the oscillator strengths at 270 nm (corresponds to 3PA coefficient) are 0.292, 0.227 and 0.174, respectively. These oscillator strengths are larger to that of the neighboured excited states as given in Table S2. Therefore, along with 2PA, there is high probability that these samples will also show 3PA in their nonlinear absorption process. In addition, from the absorption spectra [Fig. 1(a)], and DFT calculations, the HOMO-LUMO gaps (E_g) of these molecules are in the range of 3.37–3.48 eV, as mentioned in Table 3. The condition for 3PA is described as $2hv < E_g < 3hv$ [37], which is satisfied by the OA data of these molecules. Therefore, both 3 PA condition and theoretical calculations indicate that, all three molecules having RSA in nature with nonlinear absorption due to contribution of mixing of both 2PA and 3PA processes. The comparison of 3PA coefficient (α_3) with different organic samples is given in Table 6.

Optical limiting (OL) properties of these molecules can be realized from the OA Z-scan data. In OL measurement, the normalized transmittance of medium decreases at the high intensity of the beam and rises at low intensity. Therefore, for high-intensity medium behaves as a non-transparent which helps to sufficiently protect the light-sensitive components, eyes, sensors, etc from laser-induced damage [48]. This optical limiting property is used in optical limiter that attenuates the optical

Table 6
Comparison of the NLO coefficients with reported samples in literature.

Sample	Laser Parameters	$n_2 \times 10^{-16}$ (cm^2/W)	$\alpha_3 \times 10^{-5}$ (cm^3/GW^2)	Ref.
G1, G3	~70 fs, 800 nm	6.8, 7.9	4.7, 5.2	[48]
uGFPc	~70 fs, 800 nm	2.57–7.18	3.31–5.75	[37]
PN-Fb, PN-Ni, PN-Cu, PN-Zn	~70 fs, 800 nm	3.03, 3.32, 3.81, 3.87	2.68, 2.53, 2.51, 2.35	[58]
AzaPc-Pyrene in DMF	~90 fs, 800 nm	(7.06–12.85)	(10.81–10.87) $\times 10^1$	[61]
P1, P2	~190 fs, 800 nm		(3.8, 1.5) $\times 10^1$	[29]
L1, L2	~20 ps, 532 nm	8.0 $\times 10^2$		[62]
BP1, BP2, BP3	~70 fs, 800 nm	(1.87–2.79)	(6.23–7.39)	Present work

laser beams which are highly intense, potentially dangerous and allows transmittance at low intensity. Therefore, materials which exhibit RSA behaviour can be used for optical limiting studies. The most important factor in optical limiting is the optical limiting onset [49–51]. We have calculated optical limiting onset for those molecules from the OA Z-scan data. The normalized transmittance that is retrieved from the OA Z-scan and plotted with respect to input energy fluence as shown in Fig. S2. The energy fluence can be obtained from the OA Z-scan reports assuming that at z position of the sample and the fluence of the laser beam with a relationship [48].

$$E(z) = 4\sqrt{\ln 2}E_{in} \Big/ \pi^{3/2}\omega^2(z) \tag{9}$$

where E_{in} is the input energy of the laser beam and $\omega(z)$ is the beam waist at each z position of the sample. The magnitude of observed optical limiting onset is in the range of (7.78–9.02) $\times 10^{-3}$ J/cm^2, which is extrapolated with theoretical fit to experimental data, mentioned in Table S5. Ag-polymer-based nanocomposite in fs response time shows a limiting onset of about 3×10^{-2} J/cm^2 [52]. Therefore, our samples can be used as a better optical limiter as these are showing one order less than Ag- polymer nanocomposite. We have compared the optical limiting onset of different π-conjugated organic molecules and other samples with our molecules, which is mentioned in Table S5.

3.2.2. Closed-aperture (CA) Z-scan

In the CA Z-scan process, an aperture is placed in front of the detector so that the centre part of the beam after transmitting through the sample can be detected. The refractive index of material changes with intensity of incident laser beam that leads to nonlinearity in refractive index of the material [53]. For fitting the CA Z-scan data, the relation for normalized transmittance is given by the formula [48].

$$T_{CA}(x) = 1 + \frac{4x\Delta\Phi}{(1+x^2)(9+x^2)} + \frac{4(3x^2-5)\Delta\Phi^2}{(1+x^2)(9+x^2)(25+x^2)} + \frac{32(3x^2-11)x\Delta\Phi^3}{(1+x^2)(9+x^2)(25+x^2)(49+x^2)} \tag{5}$$

where T(x) is the normalized transmittance, $x = z/z_0$. z is the sample distance from focus (z = 0), $\Delta\Phi = kn_2I_0L_{eff}$ represents the on-axis phase shift at focus, n_2 specifies the nonlinear refractive index, $k = \frac{2\pi}{\lambda}$ denotes the wavenumber, $I_0 = \frac{2P}{\pi\omega_0^2}$ signifies the irradiance of the beam at focus, P is the peak power of the beam, and L_{eff} is the effective length of the sample. Therefore, $n_2 = \frac{\Delta\Phi}{kI_0L_{eff}}$, where $L_{eff} = \frac{1-e^{-\alpha_0 L}}{\alpha_0}$, α_0 and L, respectively, are the linear absorption coefficient and thickness of the sample. The nonlinear refractive index n_2 is calculated from the difference in the normalized transmittance of peak and valley using the formula [48]

$$\Delta T_{P-V} = 0.406(1-S)^{0.25}\Delta\Phi \tag{6}$$

where $S = 1 - \exp(-2r_a^2/\omega_a^2)$ is the linear transmittance of the aperture, where r_a is the radius of the aperture and ω_a is the radius of the laser spot before the aperture. The third-order susceptibility can be calculated from the nonlinear refractive index using the formula [37]

$$\left[\chi^3\right]\ (\text{esu}) = 10^{-4}\ \frac{\varepsilon_0 n_0^2 c^2}{\pi} n_2\left(\text{cm}^2/\text{W}\right) \tag{7}$$

where $\varepsilon_0 = 8.85 \times 10^{-12}\frac{N}{m}$ is the permittivity in free space, $c = 3 \times 10^8$ m/s is the velocity of light, $\lambda = 800$ nm denotes the wavelength of the laser pulse, and $n_0 = 1.42$ is the linear refractive index of the sample.

The CA Z-scan data was fitted using equation (5) and the CA curves of those molecules with removal of solvent contribution having error (± 10%) are shown in Fig. 4. (d)–(f). By fitting the data, the on-axis phase shift $\Delta\Phi$ is extracted and using the relation $\Delta\Phi = kn_2I_0L_{eff}$ nonlinear refractive index (NLR) n_2 is calculated. The evaluated magnitude of n_2 for the samples are (1.87–2.79) $\times 10^{-16}$ cm^2/W. Substituting the values of n_2 in equation (7), modulus values of third-order susceptibility are calculated with magnitude in the range, (1.0–4.43) $\times 10^{-14}$ (in esu). All the obtained values of nonlinear refractive index and third-order susceptibility for our examined molecules are mentioned in Table 5. From the experimental and fitted data, we have confirmed that all molecules show a positive NLR as the curve has a valley followed by a peak in nature and matches with mathematically calculated positive signed n_2. The comparison of n_2 of various organic and other materials obtained with different laser sources with our molecules is shown in Table 6.

The second hyperpolarizability (γ) is related to the third-order susceptibility χ^3 by the formula [54]

$$\gamma = \frac{\chi^3}{[(1/3)(n_0^2+2)]^4 N} \tag{8}$$

where n_0 denotes the linear refractive index of sample, N represents the molecular number density. Substituting the value of χ^3 in equation (8) the second hyperpolarizability was calculated. The obtained value of γ is in the range (1.97–2.96) $\times 10^{-32}$ (esu). The details of all the obtained NLO parameters are summarized in Table 5. The DFT calculated second hyperpolarizability (γ) for BP1, BP2, and BP3 are −0.12, −0.12 and −0.14 $\times 10^{-32}$ esu, respectively. The NLO properties of all the molecules are calculated by using SOS method [55]. All the molecules demonstrated with γ values in the range of 10^{-32} esu. We have compared the value of γ with some reported π-conjugated organic molecules given in Table S4. Biswas et al. studied on optical nonlinearities of π-extended thioalkyl-substituted tetrathiafulvalene sensitizers named G1, G3 using Z-scan technique with ~70 fs pulse, 800 nm laser pulses (similar experimental conditions to this work) and obtained γ values of 3.5 $\times 10^{-31}$, 4.2 $\times 10^{-31}$ esu, respectively [48]. Biswas et al. observed the linear and fs NLO properties of soluble pyrrolo [1,2-a] quinoxalines using degenerate four wave mixing technique and obtained the γ value of ~2.99-4.41 $\times 10^{-31}$ esu [56]. Kumar et al. observed values of γ ~4.27 $\times 10^{-31}$, 4.32 $\times 10^{-31}$ esu for two alkyl phthalocyanines named pc1, pc2 using DFWM technique with ~100 fs pulse, 800 nm laser [57]. Ahmed et al. reported value of γ ~ (0.7–1) $\times 10^{-31}$ esu of metalated porphyrin-Napthalimide D-A system [58]. Chen et al. reported value of γ ~1.12-3.84 $\times 10^{-32}$ esu of axially modified gallium phthalocyanines and naphthalocyanines using the Z-scan method [49]. There is some literature on the measurement of second hyperpolarizability of π-conjugated organic molecules using nanosecond pulsed laser. Shehzad et al. studied second hyperpolarizability and NLO properties of porphyrin based polyimides named NH-DATPP, Zn-PI, NH-PI, Zn-DATPP using Z-scan technique with 6 ns pulse, 532 nm ns laser and observed value of γ ~ (1.879–7.866) $\times 10^{-29}$ esu [59]. The second hyperpolarizability γ observed with in-backbone substituted oligo(triacetylene) chromophore named of space groups Dipyridophenazine, Benzothiadiazole using third-harmonic generation with 5 ns pulse, 1907 nm with a value of 0.22 $\times 10^{-33}$, 0.16 $\times 10^{-33}$ esu [60].

4. Conclusions

We reported ultrafast NLO properties of polycyclic aromatic hydrocarbon (PAHs) based benzo[e]pyrene derivatives (BP1, BP2, and BP3) using ~ 70 fs pulse duration laser with 800 nm as central wavelength. We found from the open-aperture Z-scan that all these three molecules exhibit strong reverse saturable absorption, and the nonlinear absorption dominantly originated from the mixed contribution of 2PA and 3PA. From the CA Z-scan method, we have calculated the nonlinear refractive index which is positive with valley followed by peak shape. Additionally, we calculated the second hyperpolarizability (~10^{-32} esu) which was confirmed from TDDFT theoretical calculations. From OA Z-scan transmittance data, we have calculated the optical limiting onset (~10^{-3} J/cm^2). Since these molecules depicted RSA in nature and good optical limiting onsets, we believe they will find applications in optical

limitting and optical switching.

CRediT authorship contribution statement

Sudhanshu Kumar Nayak: Data curation, Formal analysis, Investigation, Validation, Methodology, Visualization, Writing - original draft, Writing - review & editing. **Ranjith Kore:** Data curation, Formal analysis, Investigation, Validation, Methodology, Writing - original draft, Writing - review & editing. **Md Soif Ahmed:** Formal analysis, Investigation, Validation, Methodology, Writing – original draft, Writing – review & editing. **Pankaj Verma:** Data curation, Formal analysis, Investigation, Validation, Writing – review & editing, Writing – original draft. **Rohini Vallavoju:** Data curation, Formal analysis, Investigation, Validation, Writing – review & editing, Writing – original draft. **Dipanjan Banerjee:** Formal analysis, Investigation, Validation, Methodology, Writing – original draft, Writing – review & editing. **Someshwar Pola:** Conceptualization, Resources, Funding acquisition, Supervision, Formal analysis, Investigation, Validation, Methodology, Writing – original draft, Writing – review & editing. **Venugopal Rao Soma:** Conceptualization, Resources, Funding acquisition, Supervision, Formal analysis, Investigation, Validation, Methodology, Writing – original draft, Writing – review & editing. **Prabhakar Chetti:** Conceptualization, Resources, Funding acquisition, Supervision, Formal analysis, Investigation, Validation, Methodology, Writing – original draft, Writing – review & editing. **Sai Santosh Kumar Raavi:** Conceptualization, Resources, Funding acquisition, Supervision, Formal analysis, Investigation, Validation, Methodology, Writing – original draft, Writing – review & editing.

Declaration of competing interest

The authors declare that they have no known competing financial interests or personal relationships that could have appeared to influence the work reported in this paper.

Data availability

Data will be made available on request.

Acknowledgements

RSSK acknowledges the financial support for following projects on BRICS/PilotCall2/IEEE-OSC/2018 (G), and CRG/2019/003197. SKN thanks MHRD, India and IIT Hyderabad, India for financial support. D.B. acknowledge the funding support from PMRF. B. B. acknowledge DST-Inspire for fellowship. Venugopal Rao Soma thanks DRDO, India for financial support through ACRHEM.

Appendix A. Supplementary data

Supplementary data to this article can be found online at https://doi.org/10.1016/j.optmat.2023.113603.

References

[1] G. De La Torre, P. Vázquez, F. Agullo-Lopez, T. Torres, Chem. Rev. 104 (2004) 3723–3750.
[2] R.W. Boyd, Nonlinear Optics, Academic press, 2020.
[3] J. Zyss, Molecular Nonlinear Optics: Materials, Physics, and Devices, Academic press, 2013.
[4] B.E. Saleh, M.C. Teich, Fundamentals of Photonics, john Wiley & sons, 2019.
[5] J.M. Dudley, J.R. Taylor, Nat. Photonics 3 (2009) 85–90.
[6] P.N. Prasad, D.R. Ulrich, Nonlinear Optical and Electroactive Polymers, Springer Science & Business Media, 2012.
[7] W. Min, C.W. Freudiger, S. Lu, X.S. Xie, Annu. Rev. Phys. Chem. 62 (2011) 507–530.
[8] T. Sutradhar, A. Misra, RSC Adv. 10 (2020) 40300–40309.
[9] T. Sutradhar, A. Misra, ChemistrySelect 4 (2019) 3697–3705.
[10] M. Majumder, A. Misra, Phys. Chem. Chem. Phys. 20 (2018) 19007–19016.
[11] D.K. Kolmel, A. Horner, J.A. Castaneda, J.A. Ferencz, A. Bihlmeier, M. Nieger, S. Brase, L.A. Padilha, J. Phys. Chem. C 120 (2016) 4538–4545.
[12] R.L. Sutherland, Handbook of Nonlinear Optics, CRC press, 2003.
[13] J. Perry, K. Mansour, I.-Y. Lee, X.-L. Wu, P. Bedworth, C.-T. Chen, D. Ng, S. Marder, P. Miles, T. Wada, Science 273 (1996) 1533–1536.
[14] S.K. Yesodha, C.K.S. Pillai, N. Tsutsumi, Prog. Polym. Sci. 29 (2004) 45–74.
[15] Y. Wang, G.S. He, P.N. Prasad, T. Goodson, J. Am. Chem. Soc. 127 (2005) 10128–10129.
[16] G. Walters, B.R. Sutherland, S. Hoogland, D. Shi, R. Comin, D.P. Sellan, O.M. Bakr, E.H. Sargent, ACS Nano 9 (2015) 9340–9346.
[17] S. Gil-Guerrero, Á. Peña-Gallego, N. Ramos-Berdullas, A. Martin Pendas, M. Mandado, Nano Lett. 19 (2019) 7394–7399.
[18] M. Nakano, B. Champagne, J. Phys. Chem. Lett. 6 (2015) 3236–3256.
[19] M.G. Vivas, D.L. Silva, J. Malinge, M. Boujtita, R. Zaleśny, W. Bartkowiak, H. Ågren, S. Canuto, L. De Boni, E. Ishow, Sci. Rep. 4 (2014) 1–11.
[20] B.H. Cumpston, S.P. Ananthavel, S. Barlow, D.L. Dyer, J.E. Ehrlich, L.L. Erskine, A. A. Heikal, S.M. Kuebler, I.-Y.S. Lee, D. McCord-Maughon, Nature 398 (1999) 51–54.
[21] R. Chennoufi, H. Bougherara, N. Gagey-Eilstein, B. Dumat, E. Henry, F. Subra, S. Bury-Moné, F. Mahuteau-Betzer, P. Tauc, M.-P. Teulade-Fichou, Sci. Rep. 6 (2016) 1–12.
[22] Z.-M. Tang, T. Lei, J.-L. Wang, Y. Ma, J. Pei, J. Org. Chem. 75 (2010) 3644–3655.
[23] P.J. Repasky, D.a.M. Agra-Kooijman, S. Kumar, C.S. Hartley, J. Phys. Chem. B 120 (2016) 2829–2837.
[24] Z. Zhou, H.W. Qiao, Y. Hou, H.G. Yang, S. Yang, Energy Environ. Sci. 14 (2021) 127–157.
[25] B. Ivanova, M. Spiteller, Cryst. Growth Des. 10 (2010) 2470–2474.
[26] S.K. Alsaee, M.A.A. Bakar, D.A. Zainuri, A.H. Anizaim, M.F. Zaini, M.M. Rosli, M. Abdullah, S. Arshad, I.A. Razak, Opt. Mater. 128 (2022), 112314.
[27] G. Maddala, R. Gade, J. Ahemed, S. Kalvapalli, N.B. Simhachalam, P. Chetti, S. Pola, R. Mitty, Sol. Energy 226 (2021) 501–512.
[28] M. Khalid, H.M. Lodhi, M.U. Khan, M. Imran, RSC Adv. 11 (2021) 14237–14250.
[29] Z. Xiao, Y. Shi, R. Sun, J. Ge, Z. Li, Y. Fang, X. Wu, J. Yang, M. Zhao, Y. Song, J. Mater. Chem. C 4 (2016) 4647–4653.
[30] E. Cariati, C. Botta, S. Danelli, A. Forni, A. Giaretta, U. Giovanella, E. Lucenti, D. Marinotto, S. Righetto, R. Ugo, Chem. Commun. 50 (2014) 14225–14228.
[31] V.S. Puli, M. Subburu, Y. Bhongiri, A. Tripathi, K. Prasad, A. Chatterjee, S. Pola, P. Chetti, J. Mol. Struct. 1229 (2021), 129491.
[32] S. Kumar, M.-T. Ho, Y.-T. Tao, Org. Lett. 18 (2016) 4876–4879.
[33] D. O'Connor, Time-correlated Single Photon Counting, Academic press, 2012.
[34] M. Sheik-Bahae, A.A. Said, T.-H. Wei, D.J. Hagan, E.W. Van Stryland, IEEE J. Quant. Electron. 26 (1990) 760–769.
[35] C. Biswas, S.G. Palivela, L. Giribabu, V.R. Soma, S.S.K. Raavi, Opt. Mater. 127 (2022), 112232.
[36] R.S.S. Kumar, S.V. Rao, L. Giribabu, D.N. Rao, Chem. Phys. Lett. 447 (2007) 274–278.
[37] M.S. Ahmed, C. Biswas, D. Banerjee, P. Chetti, J.-S. Yang, V.R. Soma, S.S.K. Raavi, Frontiers in Physics (2022) 549.
[38] S. Raouafi, F. Aloui, J. Mol. Struct. 1196 (2019) 685–690.
[39] V.-V.V. Hugo, H.-S.M. Alejandro, V.-S.A. María, R.-H. María, L.-R.M. Antonio, P.-O. M. Guadalupe, M.-G.M. Antonio, A.-H. Fernando, A. Víctor, C.-A. Diego, Comput. Chem. 7 (2018) 1–26.
[40] E.W. Van Stryland, M. Sheik-Bahae, Z-Scan Technique for Nonlinear Materials Characterization, Materials Characterization and Optical Probe Techniques: A Critical Review, International Society for Optics and Photonics, 1997, 102910Q.
[41] A. Siahmakoun, D. Breitling, R.A. Najaf-Zadeh, Appl. Opt. 39 (2000) 5360–5366.
[42] D. Weaire, B. Wherrett, D. Miller, S. Smith, Opt Lett. 4 (1979) 331–333.
[43] D. Banerjee, S.S.B. Moram, C. Byram, J. Rathod, T. Jena, G.K. Podagatlapalli, V. R. Soma, Appl. Surf. Sci. 569 (2021), 151070.
[44] M.D. Levenson, J. Opt. Soc. Am. B 1 (1984) 409–410.
[45] N. Venkatram, D.N. Rao, L. Giribabu, S.V. Rao, Chem. Phys. Lett. 464 (2008) 211–215.
[46] C. Biswas, P.S. Gangadhar, L. Giribabu, P. Chetti, D. Banerjee, V.R. Soma, S.S. K. Raavi, J. Photochem. Photobiol. Chem. 433 (2022), 114141.
[47] S.V. Rao, D.N. Rao, J. Akkara, B. DeCristofano, D. Rao, Chem. Phys. Lett. 297 (1998) 491–498.
[48] C. Biswas, N.K. Katturi, N. Duvva, L. Giribabu, V.R. Soma, S.S.K. Raavi, J. Phys. Chem. C 124 (2020) 24039–24051.
[49] Y. Chen, M. Hanack, Y. Araki, O. Ito, Chem. Soc. Rev. 34 (2005) 517–529.
[50] L.W. Tutt, T.F. Boggess, Prog. Quant. Electron. 17 (1993) 299–338.
[51] P. Chen, I.V. Tomov, A.S. Dvornikov, M. Nakashima, J.F. Roach, D.M. Alabran, P. M. Rentzepis, J. Phys. Chem. 100 (1996) 17507–17512.
[52] N. Misra, M. Rapolu, S.V. Rao, L. Varshney, V. Kumar, Opt Laser. Technol. 79 (2016) 24–31.
[53] M.S. Ahmed, C. Biswas, P.B. Miranda, S.S.K. Raavi, Eur. Phys. J. Spec. Top. (2021) 1–17.
[54] P. Patil, S.R. Maidur, S.V. Rao, S. Dharmaprakash, Opt Laser. Technol. 81 (2016) 70–76.
[55] C. Prabhakar, K. Bhanuprakash, V.J. Rao, M. Balamuralikrishna, D.N. Rao, J. Phys. Chem. C 114 (2010) 6077–6089.
[56] C. Biswas, K. Krishnakanth, J. Lade, A. Chaskar, A. Tripathi, P. Chetti, V.R. Soma, S.S.K. Raavi, Chem. Phys. Lett. 730 (2019) 638–642.
[57] R.S.S. Kumar, S.V. Rao, L. Giribabu, D.N. Rao, Opt. Mater. 31 (2009) 1042–1047.
[58] M.S. Ahmed, C. Biswas, B. Bhavani, S. Prasanthkumar, D. Banerjee, V. Kumar, P. Chetti, L. Giribabu, V.R. Soma, S.S.K. Raavi, J. Photochem. Photobiol. Chem. 435 (2023), 114324.

[59] F.K. Shehzad, Q.U. Khan, Q. Mahmood, F. Ghafoor, H.O. Alsaab, S.A.A. Shah, N. Athir, A. Iqbal, Opt. Mater. 127 (2022), 112317.
[60] I. Biaggio, P. Günter, S. Piotto, M. Edelmann, J.-M. Raimundo, F. Diederich, JOSA B 20 (2003) 1656–1660.
[61] M. Sebastian, A. Ganesan, H. Behbehani, A. Husain, S. Makhseed, J. Phys. Chem. C 124 (2020) 21740–21750.
[62] P. Liang, Z. Li, Y. Mi, Z. Yang, D. Wang, H. Cao, W. He, H. Yang, J. Electron. Mater. 44 (2015) 2883–2889.